 Printed in China Communications in Theoretical Physics

Commun. Theor. Phys. **77** (2025) 035302 (9pp) https://doi.org/10.1088/1572-9494/ad8dba

Re-examination of the β-decay properties of As isotopes

Abdul Kabir[1], **Jameel-Un Nabi**[2], **Wajeeha Khalid**[2] **and Hamad Almujibah**[3]

[1] Department of Space Science, Institute of Space Technology, Islamabad 44000, Pakistan
[2] University of Wah, Quaid Avenue, Wah Cantt 47040, Punjab, Pakistan
[3] Department of Civil Engineering, College of Engineering, Taif University, PO Box 11099, Taif 21974, Saudi Arabia

E-mail: kabirkhanak1@gmail.com

Received 19 July 2024, revised 30 October 2024
Accepted for publication 31 October 2024
Published 12 December 2024

Abstract

The β-decay properties of $^{67-80}$As nuclei have been investigated within the framework of the proton–neutron quasi-particle random phase approximation (pn-QRPA) model. The nuclear deformation obtained from the finite range droplet model is used as an input parameter in the pn-QRPA model for the analysis of β-decay properties including Gamow–Teller strength distributions, log *ft*, β-decay half-lives and stellar $\beta^{\pm}$ decay rates. The predicted log *ft* values were fairly consistent with the observed data. The computed β-decay half-lives matched the measured values by a factor of 10. The stellar rates were compared with the shell model outcomes. At high densities and temperatures, the β^{+} and electron capture rates had a finite contribution. However, the β^{-} and positron capture rates are only significant at high temperatures and low densities. The pn-QRPA rates outperformed the shell model rates by a factor of 22 or more.

Supplementary material for this article is available online

Keywords: pn-QRPA, β-decay properties, GT strength distribution, log *ft*, stellar rates

1. Introduction

Accurate measurements and reliable theoretical calculations of the properties of low-energy nuclear structure play a vital role in the modeling and comprehension of fundamental nuclear phenomena. These include β-decays, which are closely linked to stellar nucleosynthesis. The β-decay characteristics are calculated from the perspective of theory, and so serve as a standard for theoretical models as they are sensitive to the wave functions in the parent and daughter states. The unique features of low-lying excitation energies and decay patterns found in neutron-rich nuclei around $A = 100$ and possessing $N \approx 60$ are especially intriguing, holding importance for both studies of nuclear structure and astrophysical investigations [1, 2]. In these nuclei, shape dynamics may occur. Furthermore, these properties contribute to the rapid neutron capture (r-) process, which accounts for the production of heavy elements via nucleosynthesis in explosive scenarios. The r-process is responsible for producing around 50% of the nuclei that are more massive than iron [3, 4]. Radioactive ion beams are widely used in major experimental facilities across the world to accurately measure the β-decay half-lives of neutron-rich nuclei. Researchers have studied the β-decay properties of several neutron-rich nuclei including Ge and As [5–7]. Due to limited data from experiments, theoretical models have been used to study the β-decay rates of neutron-rich nuclei. Theoretical attempts to define low-lying nuclear states and their decay properties have encountered substantial difficulties. The decay process has been studied theoretically utilizing several nuclear models. A few models that are often utilized to accomplish these computations include the interacting boson model (IBM) [8], the quasi-particle random phase approximation (QRPA) [9, 10], the large-scale shell model (LSSM) [11] and the potential model [12, 13]. The structure of odd-*A* energy levels and the electromagnetic properties of ^{69,71,73}As and ^{69,71,73}Ge were studied in the context of the proton–neutron interacting boson–fermion model (pn-IBFM) [14]. Furthermore, the β-decay properties of neutron-rich nuclei have been studied by employing the deformed pn-QRPA [15]. The impact of finite-range tensor forces for even–even semi-magic/magic nuclei on the low-lying Gamow–Teller (GT) state and β-decay half-lives [16–19]. The β-decay and electron capture

(EC) rates of Mn isotopes in the mass range $A = 53$–63 have been determined using the pn-QRPA [20]. The nuclear structural characteristics and β-decay half-lives of exotic proton-rich waiting point nuclei in the mass range $A \approx 70$ have been examined using both the pn-QRPA and the interacting boson model-1 (IBM-1) [21].

Using a microscopic nuclear theory, Klapdor-Kleingrothaus *et al* [22] were the first to determine β-decay rates for several nuclei that are far from the line of stability. Later, this framework was employed to compute the β-decay half-lives of over 6000 nuclei rich in neutrons, spanning a wide range from the line of stability to the neutron drip line [23]. A microscopic computation of the β^+/electron capture rates of neutron-deficient nuclei with $Z = 10$–108, up to the proton drip line for over 2000 nuclei, was performed using the same pn-QRPA model, which has a separable and schematic interaction [24]. The modest interaction rates have greatly aided our comprehension of the r-process. Fuller *et al* [25] calculated rates at stellar temperatures and densities, focusing on decays from excited states of parent nuclei. We utilize the deformed basis pn-QRPA models to provide a reliable description of the nuclear structure and β-decay properties of As isotopes. The proposed model is capable of finding the β-decay properties [26] and microscopic calculation of weak rates for any arbitrary heavy nucleus [27, 28].

We have investigated the β-decay properties of selected As isotopes (including the terrestrial β-decay half-lives, GT strength distributions, log *ft* values and stellar rates) by focusing on their dependence on deformation by employing the theoretical framework of the deformed pn-QRPA model. The β-decay properties for each As isotope were analyzed as a function of the quadrupole deformation parameter β_2. In isotopes with mass numbers between 67 and 80 there exist prolate, spherical and oblate shapes, corresponding to $\beta > 0$, $\beta = 0$ and $\beta < 0$, respectively. Particular characteristics may be seen in the β-decay properties computed at each equilibrium deformation. The goal of this study is to identify possible indicators of nuclear shape in the β-decay characteristics of As nuclei within $67 \leqslant A \leqslant 80$. The results of the present model-based analysis were compared with previously observed and predicted data.

The paper is arranged as follows. In section 2, we give a brief discussion of the pn-QRPA model used to compute nuclear structure and β-decay features. Section 3 offers our findings and pertinent discussion. Section 4 summarizes the results of the present examination.

2. Formalism

The pn-QRPA model was used to study the β-decay characteristics of As nuclei. The Hamiltonian of the pn-QRPA model can be described using

$$\mathscr{H}^{\mathrm{QRPA}} = \mathscr{H}^{\mathrm{sp}} + \mathscr{V}^{\mathrm{pair}} + \mathscr{V}^{\mathrm{pp}}_{\mathrm{GT}} + \mathscr{V}^{\mathrm{ph}}_{\mathrm{GT}}. \tag{1}$$

The Hamiltonian for a single particle is denoted as $\mathscr{H}^{\mathrm{sp}}$, while $\mathscr{V}^{\mathrm{pair}}$ represents the interaction between nucleons. The term $\mathscr{V}^{\mathrm{pp}}_{\mathrm{GT}}$ corresponds to the particle–particle (pp) interactions and $\mathscr{V}^{\mathrm{ph}}_{\mathrm{GT}}$ corresponds to the particle–hole (ph) GT interactions. The wave functions and energy of a single particle were determined utilizing the Nilsson model [29]. The oscillator constant for the nucleon was calculated as $\hbar\omega = (45A^{-1/3} - 25A^{-2/3})$. Other variables associated with the model include β_2, pairing gaps, Nilsson potential parameters (NPP), GT force variables and Q-values. The NPP was modified from [30] and Q-values were obtained using mass excess values [31]. To get proton and neutron quasi-particle energies and occupancy probability, the BCS computations were solved with pairing gaps obtained utilizing the relation.

$$\begin{aligned}\Delta_{\mathrm{nn}} = \frac{1}{8}(-1)^{A-Z+1}[2S_{\mathrm{n}}(A+1, Z) \\ - 4S_{\mathrm{n}}(A, Z) + 2S_{\mathrm{n}}(A-1, Z)],\end{aligned} \tag{2}$$

$$\begin{aligned}\Delta_{\mathrm{pp}} = \frac{1}{8}(-1)^{1+Z}[2S_{\mathrm{p}}(A+1, Z+1) \\ - 4S_{\mathrm{p}}(A, Z) + 2S_{\mathrm{p}}(A-1, Z-1)],\end{aligned} \tag{3}$$

where S_{p} is the proton separation energy and S_{n} is the neutron separation energy. The current pn-QRPA model has the limitation of ignoring the p–n pairing effect, and incorporation of p–n pairing may be the topic of future work. The present paper included the nn and pp pairing correlations, which have only an isovector contribution. For the isoscalar (IS) part, one must include the p–n pairing correlations, which was not considered in the present manuscript. The conclusions of the study in [32] state that IS interaction behaves in a way like the tensor force (TF) interaction. The study was performed only for $N = Z + 2$ nuclei. The IS interaction may impact the GT computation in a way similar to that of TF interaction, provided that the conclusions of the study can be generalized to any arbitrary nucleus (including $N = Z$). The calculations of [32] showed that TF shifts the GT peak to low excitation energies. Incorporation of TF may result in lower centroid values of calculated GT strength distributions and could lead to higher values of calculated β-decay rates. The same effect of shifting calculated β-strength to lower excitation energies in the current pn-QRPA model was achieved by incorporation of particle–particle forces [24]. To summarize, our model has the shortcoming of not incorporating the p–n pairing effect. The pp forces in the GT residual interaction take care of this missing effect.

The β_2 values were obtained from [33]. The GT force parameters were taken from [34]. For details of the pairing force and residual interaction as well as solution of equation (1) one can consult [35].

The partial half-lives $t_{1/2}$ and log *ft* were determined as

$$t_{1/2} = \frac{C}{(g_{\mathrm{A}}/g_{\mathrm{V}})^2 f_{\mathrm{A}}(A, Z, E) B_{\mathrm{GT}}(\omega) + f_{\mathrm{V}}(A, Z, E) B_{\mathrm{F}}(\omega)}, \tag{4}$$

$$\log ft = \log \frac{C}{B_{\mathrm{GT}}(\omega) + B_{\mathrm{F}}(\omega)}, \tag{5}$$

where $C = 6143$ s [36]. The ratio $g_A/g_V = -1.2694$ [37], $E = (Q - \omega)$ and Q was taken from [31]. ω is the excitation energy of the QRPA phonon determined by solving the random phase approximation matrix equation. $f_{\mathrm{V}}(A, Z, E)$ is the phase space factor for the vector transitions and $f_{\mathrm{A}}(A, Z, E)$ is

Table 1. Modes of terrestrial decay and pn-QRPA model parameters for $^{67-80}$As (EC, electron capture).

Nucleus	Decay mode	Q_β (MeV)	β_2	Δ_{pp} (MeV)	Δ_{nn} (MeV)
^{67}As	β^+	6.0868	0.2200	1.6478	0.4330
^{68}As	β^+	8.0843	−0.2870	1.0123	1.0407
^{69}As	β^+	3.9907	−0.2970	1.6642	1.2249
^{70}As	β^+	6.2280	−0.2670	1.0901	1.3316
^{71}As	β^+	2.0137	−0.2580	1.6368	1.3892
^{72}As	β^+	4.3559	−0.2580	1.0867	1.4020
^{73}As	EC	0.3445	−0.2380	1.7432	1.3004
^{74}As	β^+	2.5623	−0.2380	1.2233	1.2707
^{75}As	Stable	−0.8647	−0.2380	1.6793	1.2959
^{76}As	β^-	2.9605	−0.2480	1.3112	1.3211
^{77}As	β^-	0.6832	0.1730	1.6137	1.2729
^{78}As	β^-	4.2089	0.1730	1.2021	1.1606
^{79}As	β^-	2.2814	0.1740	1.6112	1.0395
^{80}As	β^-	5.5445	0.1730	1.1574	0.9948

the phase space integrals for the axial vector transitions. The phase space integrals contains the lepton kinematics. These were analyzed utilizing the formula mentioned in [38]. B_{GT} is the reduced GT transition probability and B_F is the reduced GT Fermi transition probability. The β-decay terrestrial half-lives were computed by adding up the inverses of the partial half-lives and taking the inverse

$$T_{1/2} = \left(\sum_{0 \leqslant \omega \leqslant Q} \left(\frac{1}{t_{1/2}} \right) \right)^{-1}. \tag{6}$$

From parent level n to daughter state m, the stellar weak rate was calculated utilizing

$$\lambda_{mn}^{\beta^\pm/\mathrm{EC/PC}} = \ln 2 \frac{f_{mn}^{\beta^\pm/\mathrm{EC/PC}}(\rho, T, E_f)}{(ft)_{mn}}. \tag{7}$$

One may view more information on the solution to equation (1) in [39, 40]. The sum of the stellar rates was calculated using

$$\lambda^{\beta^\pm/\mathrm{EC/PC}} = \sum_{mn} P_m \lambda_{mn}^{\beta^\pm/\mathrm{EC/PC}}, \tag{8}$$

where P_m, which was calculated using the Boltzmann distribution, is the occupancy probability of the parent excited state. We continued to sum the initial and final states until our rate computation reached the necessary degree of convergence.

3. Results and discussion

The pn-QRPA model was applied to examine the β-decay half-lives of $^{67-80}$As nuclei. Table 1 displays the terrestrial decay modes, Q-values [31], deformation parameters β_2 and pairing gap values for $^{67-80}$As. Q-values drop for odd-A and odd–odd isotopes for β^+ decay as the mass number increases. The Q-values begin to rise in the β^- direction for both the odd-A and odd–odd isotopes of As once they pass the stable ^{75}As nucleus. Self-consistent calculations of the β-decay

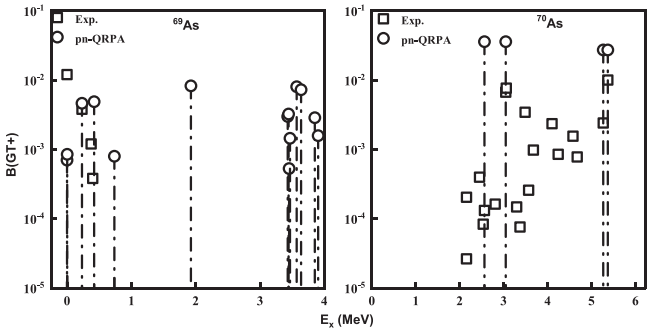

Figure 1. Comparison of the pn-QRPA-calculated GT strength distributions of ^{69}As and ^{70}As with experimental data [41, 42]. The abscissa shows daughter excitation energy within the Q-window.

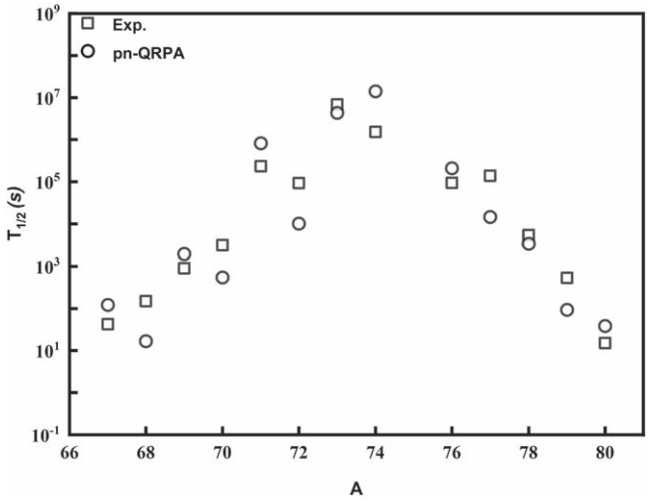

Figure 2. Comparison of the pn-QRPA-calculated half-lives of As isotopes with experimental data [31].

characteristics were performed utilizing the pn-QRPA model with the nuclear deformations obtained from [33] as an input parameter.

Figure 1 compares the pn-QRPA-predicted GT+ strength with outcomes from experiments [41, 42] for ^{69,70}As isotopes. The measured data were accessible up to excitation energies of 0.39 MeV and 5.37 MeV for ^{69}As and ^{70}As, respectively. We have also shown the calculated GT distributions inside the cut-off energies (3.99 MeV for ^{69}As and 6.22 MeV for ^{70}As). The low-lying transitions are consistent with the observed data for ^{69}As. The observed data for the decay of ^{70}As range from 2.0 MeV to 5.5 MeV. The predicted GT distributions are not considerably split for the case of ^{70}As. The present pn-QRPA model only analyzes 1p–1h correlations. Figure 1 demonstrates that the pn-QRPA-predicted GT strength distributions are more consistent with the experimental data at lower excitation energies.

Figure 2 compares the pn-QRPA calculated half-lives with the measured data of [31] for the selected As isotopes. It is obvious that high GT intensities cause low values of half-life and vice versa. It is clear from figure 1 that for odd–odd cases the GT intensities are maximum, so for the odd–odd cases the β-decay half-lives are minimum. Figure 3 displays

Table 2. An examination of predicted and observed [43] log *ft* values for β^+/EC decays of odd-*A* As isotopes. The last three columns display the predictions via pn-QRPA, IBFM-2 [18] and IBFM-2-SCMF [44], respectively.

		log *ft*			
Decay	$I_i \rightarrow I_f$	Exp. [43]	pn-QRPA	IBFM-2 [18]	IBFM-2-SCMF [44]
$^{67}As \rightarrow {}^{67}Ge$	$5/2^-_1 \rightarrow 5/2^-_1$	5.44	6.10	—	4.15
	$5/2^-_1 \rightarrow 5/2^-_2$	5.92	5.62	—	6.63
	$5/2^-_1 \rightarrow 5/2^-_3$	6.40	5.89	—	6.08
	$5/2^-_1 \rightarrow 3/2^-_1$	6.18	6.04	—	6.49
	$5/2^-_1 \rightarrow 3/2^-_2$	5.64	8.58	—	7.61
$^{69}As \rightarrow {}^{69}Ge$	$5/2^-_1 \rightarrow 5/2^-_1$	5.49	6.74	4.26	4.77
	$5/2^-_1 \rightarrow 5/2^-_2$	6.94	6.65	6.65	6.92
	$5/2^-_1 \rightarrow 5/2^-_3$	6.80	5.91	5.33	5.63
	$5/2^-_1 \rightarrow 5/2^-_4$	6.47	5.89	5.49	5.98
	$5/2^-_1 \rightarrow 5/2^-_5$	5.95	6.68	—	7.15
	$5/2^-_1 \rightarrow 3/2^-_1$	6.05	5.66	5.88	7.58
	$5/2^-_1 \rightarrow 3/2^-_2$	7.21	6.10	7.90	7.44
	$5/2^-_1 \rightarrow 3/2^-_3$	6.71	6.07	5.07	6.43
	$5/2^-_1 \rightarrow 3/2^-_4$	5.82	6.86	6.46	7.07
	$5/2^-_1 \rightarrow 3/2^-_5$	6.21	6.42	6.73	8.00
	$5/2^-_1 \rightarrow 7/2^-_1$	6.20	5.68	7.54	10.85
	$5/2^-_1 \rightarrow 7/2^-_2$	—	5.72	—	7.46
$^{71}As \rightarrow {}^{71}Ge$	$5/2^-_1 \rightarrow 5/2^-_1$	5.85	7.63	4.60	5.92
	$5/2^-_1 \rightarrow 5/2^-_2$	—	7.33	6.08	6.28
	$5/2^-_1 \rightarrow 5/2^-_3$	6.86	6.59	5.63	6.55
	$5/2^-_1 \rightarrow 5/2^-_4$	9.14	7.80	5.55	7.74
	$5/2^-_1 \rightarrow 5/2^-_5$	6.96	6.98	—	6.84
	$5/2^-_1 \rightarrow 3/2^-_1$	7.19	6.05	6.52	6.74
	$5/2^-_1 \rightarrow 3/2^-_2$	>8.60	6.83	7.79	7.47
	$5/2^-_1 \rightarrow 3/2^-_3$	6.33	6.83	5.73	7.24
	$5/2^-_1 \rightarrow 3/2^-_4$	7.43	6.83	5.21	8.25
	$5/2^-_1 \rightarrow 3/2^-_5$	6.94	6.54	7.34	8.10
	$5/2^-_1 \rightarrow 7/2^-_1$	8.79	6.54	7.6	8.38
	$5/2^-_1 \rightarrow 7/2^-_2$	7.29	6.54	—	7.85
$^{73}As \rightarrow {}^{73}Ge$	$3/2^-_1 \rightarrow 1/2^-_1$	5.40	5.33	—	3.82

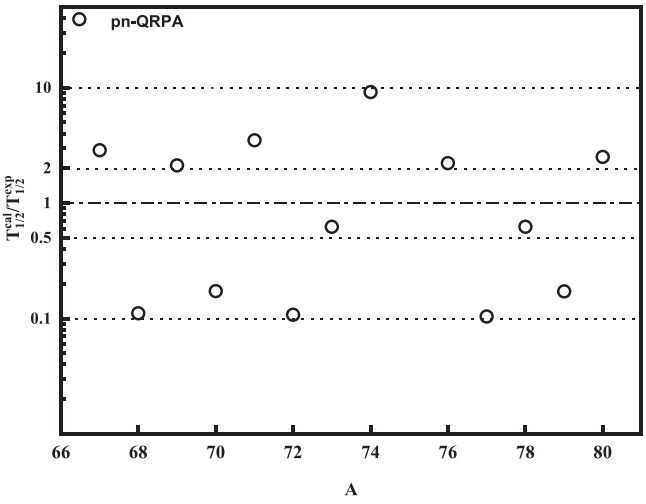

Figure 3. Ratio of the calculated to measured [31] half-lives for As isotopes.

Table 3. An examination of predicted and observed [43] log *ft* values for β^+/EC decays of odd–odd As isotopes. The last two columns display theoretical values predicted with the pn-QRPA, and IBFM-2-SCMF [44] models, respectively.

			log *ft*	
Decay	$I_i \rightarrow I_f$	Exp. [43]	pn-QRPA	IBFM-2-SCMF [44]
$^{68}As \rightarrow {}^{68}Ge$	$3^+_1 \rightarrow 2^+_1$	7.38	4.64	6.66
	$3^+_1 \rightarrow 2^+_2$	6.86	4.53	6.95
	$3^+_1 \rightarrow 2^+_3$	6.89	4.37	6.34
	$3^+_1 \rightarrow 2^+_4$	7.24	4.23	5.81
	$3^+_1 \rightarrow 2^+_5$	6.57	5.41	7.21
	$3^+_1 \rightarrow 4^+_1$	7.02	5.86	6.34
	$3^+_1 \rightarrow 4^+_2$	6.74	5.58	5.73
	$3^+_1 \rightarrow 4^+_3$	5.97	4.82	6.63
$^{70}As \rightarrow {}^{70}Ge$	$4^+_1 \rightarrow 4^+_1$	7.30	6.38	6.58
	$4^+_1 \rightarrow 4^+_2$	7.37	6.40	6.03
	$4^+_1 \rightarrow 4^+_3$	5.69	4.77	6.01
	$4^+_1 \rightarrow 3^+_1$	6.97	6.05	10.74

Table 4. Calculated sum of β^+ and EC stellar rates for As isotopes as a function of core temperature and density values in units of s^{-1}. The temperatures (T_9) and densities (ρ) are given in units of 10^9 K and g cm^{-3}, respectively. Calculated rates are compared with the previous IPM-03 calculation [46].

		^{67}As		^{68}As		^{69}As	
ρ	T_9	$\lambda^{(\beta^+ + EC)}_{pn-QRPA}$	$\lambda^{(\beta^+ + EC)}_{IPM-03}$ [46]	$\lambda^{(\beta^+ + EC)}_{pn-QRPA}$	$\lambda^{(\beta^+ + EC)}_{IPM-03}$ [46]	$\lambda^{(\beta^+ + EC)}_{pn-QRPA}$	$\lambda^{(\beta^+ + EC)}_{IPM-03}$ [46]
10^3	3	2.56×10^{-02}	6.49×10^{-02}	7.95×10^{-02}	5.37×10^{-02}	4.60×10^{-03}	8.61×10^{-03}
	10	$1.06 \times 10^{+00}$	8.50×10^{-01}	$2.71 \times 10^{+00}$	7.10×10^{-01}	3.47×10^{-01}	4.19×10^{-01}
	30	$8.84 \times 10^{+02}$	$2.48 \times 10^{+02}$	$1.36 \times 10^{+03}$	$4.46 \times 10^{+02}$	$4.11 \times 10^{+02}$	$1.84 \times 10^{+02}$
10^7	3	6.26×10^{-02}	$9.39 \times 10^{+02}$	2.04×10^{-01}	1.02×10^{-01}	2.68×10^{-02}	4.44×10^{-02}
	10	$1.28 \times 10^{+00}$	$1.01 \times 10^{+00}$	$3.28 \times 10^{+00}$	8.31×10^{-01}	4.29×10^{-01}	5.15×10^{-01}
	30	$8.90 \times 10^{+02}$	$2.50 \times 10^{+02}$	$1.37 \times 10^{+03}$	$4.49 \times 10^{+02}$	$4.14 \times 10^{+02}$	$1.85 \times 10^{+02}$
10^{11}	3	$7.43 \times 10^{+04}$	$6.43 \times 10^{+04}$	$1.26 \times 10^{+05}$	$5.45 \times 10^{+04}$	$8.02 \times 10^{+04}$	$4.80 \times 10^{+04}$
	10	$1.81 \times 10^{+05}$	$6.85 \times 10^{+04}$	$3.08 \times 10^{+05}$	$5.71 \times 10^{+04}$	$1.11 \times 10^{+05}$	$4.98 \times 10^{+04}$
	30	$6.50 \times 10^{+05}$	$1.13 \times 10^{+05}$	$8.91 \times 10^{+05}$	$1.77 \times 10^{+05}$	$3.53 \times 10^{+05}$	$8.67 \times 10^{+04}$

		^{70}As		^{71}As		^{72}As	
ρ	T_9	$\lambda^{(\beta^+ + EC)}_{pn-QRPA}$	$\lambda^{(\beta^+ + EC)}_{IPM-03}$ [46]	$\lambda^{(\beta^+ + EC)}_{pn-QRPA}$	$\lambda^{(\beta^+ + EC)}_{IPM-03}$ [46]	$\lambda^{(\beta^+ + EC)}_{pn-QRPA}$	$\lambda^{(\beta^+ + EC)}_{IPM-03}$ [46]
10^3	3	2.27×10^{-02}	8.48×10^{-03}	1.75×10^{-04}	3.63×10^{-04}	4.08×10^{-04}	8.60×10^{-04}
	10	$1.61 \times 10^{+00}$	3.12×10^{-01}	1.06×10^{-01}	1.81×10^{-01}	3.18×10^{-01}	1.35×10^{-01}
	30	$1.40 \times 10^{+03}$	$3.17 \times 10^{+02}$	$2.28 \times 10^{+02}$	$1.01 \times 10^{+02}$	$5.13 \times 10^{+02}$	$2.02 \times 10^{+02}$
10^7	3	1.33×10^{-01}	3.98×10^{-02}	4.23×10^{-03}	1.18×10^{-02}	9.75×10^{-03}	1.21×10^{-02}
	10	$1.98 \times 10^{+00}$	4.29×10^{-04}	1.32×10^{-01}	2.23×10^{-01}	3.96×10^{-01}	1.67×10^{-01}
	30	$1.41 \times 10^{+03}$	$3.19 \times 10^{+02}$	$2.30 \times 10^{+02}$	$1.02 \times 10^{+02}$	$5.18 \times 10^{+02}$	$2.04 \times 10^{+02}$
10^{11}	3	$1.96 \times 10^{+05}$	$3.54 \times 10^{+04}$	$5.21 \times 10^{+04}$	$2.34 \times 10^{+04}$	$8.36 \times 10^{+04}$	$1.78 \times 10^{+04}$
	10	$3.69 \times 10^{+05}$	$3.61 \times 10^{+04}$	$7.98 \times 10^{+04}$	$2.46 \times 10^{+04}$	$1.82 \times 10^{+05}$	$1.82 \times 10^{+04}$
	30	$1.15 \times 10^{+06}$	$1.27 \times 10^{+05}$	$2.52 \times 10^{+05}$	$4.91 \times 10^{+04}$	$5.53 \times 10^{+05}$	$8.07 \times 10^{+04}$

		^{73}As		^{74}As		^{75}As	
ρ	T_9	$\lambda^{(\beta^+ + EC)}_{pn-QRPA}$	$\lambda^{(\beta^+ + EC)}_{IPM-03}$ [46]	$\lambda^{(\beta^+ + EC)}_{pn-QRPA}$	$\lambda^{(\beta^+ + EC)}_{IPM-03}$ [46]	$\lambda^{(\beta^+ + EC)}_{pn-QRPA}$	$\lambda^{(\beta^+ + EC)}_{IPM-03}$ [46]
10^3	3	1.34×10^{-05}	$3.52 \times 10^{+04}$	2.22×10^{-05}	2.86×10^{-04}	1.32×10^{-07}	3.29×10^{-07}
	10	3.03×10^{-02}	4.84×10^{-02}	1.16×10^{-01}	1.34×10^{-01}	8.43×10^{-03}	1.46×10^{-02}
	30	$1.75 \times 10^{+02}$	$6.36 \times 10^{+01}$	$4.60 \times 10^{+02}$	$1.46 \times 10^{+02}$	$1.44 \times 10^{+02}$	$4.60 \times 10^{+01}$
10^7	3	4.75×10^{-04}	1.12×10^{-03}	8.95×10^{-04}	9.87×10^{-03}	6.47×10^{-06}	1.67×10^{-05}
	10	3.79×10^{-02}	6.02×10^{-02}	1.45×10^{-01}	1.67×10^{-01}	1.06×10^{-02}	1.83×10^{-02}
	30	$1.76 \times 10^{+02}$	$6.40 \times 10^{+01}$	$4.65 \times 10^{+02}$	$1.47 \times 10^{+02}$	$1.45 \times 10^{+02}$	$4.63 \times 10^{+01}$
10^{11}	3	$3.98 \times 10^{+04}$	$1.47 \times 10^{+04}$	$7.29 \times 10^{+04}$	$1.87 \times 10^{+04}$	$3.53 \times 10^{+04}$	$1.22 \times 10^{+04}$
	10	$5.81 \times 10^{+04}$	$1.49 \times 10^{+04}$	$1.81 \times 10^{+05}$	$1.91 \times 10^{+04}$	$5.43 \times 10^{+04}$	$1.24 \times 10^{+04}$
	30	$2.43 \times 10^{+05}$	$3.22 \times 10^{+04}$	$6.15 \times 10^{+05}$	$6.21 \times 10^{+04}$	$2.42 \times 10^{+05}$	$2.58 \times 10^{+04}$

		^{76}As		^{77}As		^{78}As	
ρ	T_9	$\lambda^{(\beta^+ + EC)}_{pn-QRPA}$	$\lambda^{(\beta^+ + EC)}_{IPM-03}$ [46]	$\lambda^{(\beta^+ + EC)}_{pn-QRPA}$	$\lambda^{(\beta^+ + EC)}_{IPM-03}$ [46]	$\lambda^{(\beta^+ + EC)}_{pn-QRPA}$	$\lambda^{(\beta^+ + EC)}_{IPM-03}$ [46]
10^3	3	1.77×10^{-07}	1.63×10^{-05}	1.00×10^{-09}	1.76×10^{-09}	1.23×10^{-14}	4.84×10^{-07}
	10	2.69×10^{-02}	5.41×10^{-02}	1.83×10^{-03}	3.67×10^{-03}	1.41×10^{-03}	1.33×10^{-02}
	30	$3.27 \times 10^{+02}$	$1.01 \times 10^{+02}$	$1.26 \times 10^{+02}$	$3.16 \times 10^{+01}$	$2.69 \times 10^{+02}$	$6.16 \times 10^{+01}$
10^7	3	8.93×10^{-06}	7.43×10^{-04}	5.13×10^{-08}	9.12×10^{-08}	6.38×10^{-13}	2.43×10^{-05}
	10	3.37×10^{-02}	6.77×10^{-02}	2.30×10^{-03}	4.59×10^{-03}	1.77×10^{-03}	1.67×10^{-02}
	30	$3.30 \times 10^{+02}$	$1.02 \times 10^{+02}$	$1.27 \times 10^{+02}$	$3.18 \times 10^{+01}$	$2.71 \times 10^{+02}$	$6.22 \times 10^{+01}$
10^{11}	3	$9.25 \times 10^{+04}$	$1.59 \times 10^{+04}$	$2.72 \times 10^{+04}$	$9.89 \times 10^{+03}$	$6.04 \times 10^{+04}$	$1.22 \times 10^{+04}$
	10	$1.84 \times 10^{+05}$	$1.62 \times 10^{+04}$	$4.42 \times 10^{+04}$	$9.93 \times 10^{+03}$	$1.58 \times 10^{+05}$	$1.25 \times 10^{+04}$
	30	$5.53 \times 10^{+05}$	$4.65 \times 10^{+04}$	$2.33 \times 10^{+05}$	$1.98 \times 10^{+4}$	$5.38 \times 10^{+05}$	$3.18 \times 10^{+04}$

Table 4. (Continued.)

		^{79}As		^{80}As	
ρ	T_9	$\lambda^{(\beta^+ + \mathrm{EC})}_{\mathrm{pn-QRPA}}$	$\lambda^{(\beta^+ + \mathrm{EC})}_{\mathrm{IPM-03}}$ [46]	$\lambda^{(\beta^+ + \mathrm{EC})}_{\mathrm{pn-QRPA}}$	$\lambda^{(\beta^+ + \mathrm{EC})}_{\mathrm{IPM-03}}$ [46]
		^{79}As		^{80}As	
ρ	T_9	$\lambda^{(\beta^+ + \mathrm{EC})}_{\mathrm{pn-QRPA}}$	$\lambda^{(\beta^+ + \mathrm{EC})}_{\mathrm{IPM-03}}$ [46]	$\lambda^{(\beta^+ + \mathrm{EC})}_{\mathrm{pn-QRPA}}$	$\lambda^{(\beta^+ + \mathrm{EC})}_{\mathrm{IPM-03}}$ [46]
10^3	3	3.04×10^{-12}	9.73×10^{-12}	1.48×10^{-12}	4.94×10^{-09}
	10	6.87×10^{-04}	9.94×10^{-04}	2.03×10^{-03}	3.96×10^{-03}
	30	$1.33 \times 10^{+02}$	$2.23 \times 10^{+01}$	$2.74 \times 10^{+02}$	$4.01 \times 10^{+01}$
10^7	3	1.56×10^{-10}	5.06×10^{-10}	7.66×10^{-11}	2.56×10^{-07}
	10	8.63×10^{-04}	1.25×10^{-03}	2.55×10^{-03}	4.97×10^{-03}
	30	$1.34 \times 10^{+02}$	$2.25 \times 10^{+01}$	$2.77 \times 10^{+02}$	$4.04 \times 10^{+01}$
10^{11}	3	$3.04 \times 10^{+04}$	$8.00 \times 10^{+03}$	$5.46 \times 10^{+04}$	$1.06 \times 10^{+04}$
	10	$5.25 \times 10^{+04}$	$8.20 \times 10^{+03}$	$1.51 \times 10^{+05}$	$1.07 \times 10^{+04}$
	30	$2.56 \times 10^{+05}$	$1.58 \times 10^{+04}$	$5.27 \times 10^{+05}$	$2.38 \times 10^{+04}$

the ratios of pn-QRPA computed to measured half-lives. The calculated half-lives are reproduced within a factor of 10 of the measured half-lives. This indicates good accuracy of the underlying nuclear model. The pn-QRPA model accurately predicts β-decay half-lives for neutron-rich nuclei.

Table 2 compares the pn-QRPA-based computed log *ft* for β^+/EC of odd-*A* As nuclei with those of observed data [43] and earlier predictions [pn-IBFM-2 [18] and self-consistent mean-field (IBFM-2-SCMF) calculations [44]]. The pn-QRPA-based calculated log *ft* values correlate well with the observed data. For most transitions, the IBFM-2 predictions are lower than the measured values. The log *ft* values estimated by the IBFM-2-SCMF model, which are sensitive to the wave functions for the initial and final states, were consistently greater than the IBFM-2 values. The largest deviation occurs, for example, in the case of $^{67}\mathrm{As}(5/2^+_1) \rightarrow {}^{67}\mathrm{Ge}(3/2^+_2)$ decay. In particular, the computed log *ft* is a factor of 1.52 larger than the experimental data because pn-QRPA predicted a GT strength as small as 0.000 01. The agreement with the experimental data was evaluated through the calculation of root mean square (rms) errors. The rms error for the present pn-QRPA-based prediction is 1.06 while for IBFM-2 and IBFM-2-SCMF the rms errors are 1.34 and 1.31, respectively. This indicates that pn-QRPA predictions are within the range of observed values. The IBFM-2 framework relies significantly on empirical variables for the even–even IBM-2 core Hamiltonian. As a result, phenomenological single-particle energies were employed in the IBFM-2 computation. The IBFM-2-SCMF model utilized energy density functional computations to estimate the majority of the parameters.

Similarly, table 3 compares predicted and observed log *ft* values for β^+/EC transitions of odd–odd As nuclei. The IBFM-2 model was not capable of computing the log *ft* values for odd–odd nuclei. For the decay $^{68}\mathrm{As} \rightarrow {}^{68}\mathrm{Ge}$, our calculated log *ft* values are smaller than the measured ones. This is due to the fact that GT intensities are comparatively higher, which inversely affects the half-lives and the log *ft* values. The pn-QRPA-calculated log *ft* are within the limit of measured data for ^{70}As. For example, the greatest discrepancy exists in the case of the $^{68}\mathrm{Ge}(3^+_1) \rightarrow {}^{68}\mathrm{As}(2^+_4)$ decay. In particular, the computed log *ft* is a factor of 1.71 smaller than the measured value. This is because the pn-QRPA-predicted the GT strength to be larger than 0.226 30. More fragmentations occur in this decay. The rms errors for pn-QRPA and IBFM-2-SCMF are 1.76 and 1.34, respectively.

The time derivative of the lepton-to-baryon ratio Y_e is an important quantity to keep track of throughout the pre-supernova evolution of a massive star. It is provided by

$$\dot{Y}_e^{(\beta^- + \mathrm{PC})} = \frac{\tau}{A} \lambda^{(\beta^- + \mathrm{PC})}, \tag{9}$$

$$\dot{Y}_e^{(\beta^+ + \mathrm{EC})} = -\frac{\tau}{A} \lambda^{(\beta^+ + \mathrm{EC})}, \tag{10}$$

where τ represents the abundance of the nucleus and A represents its mass number. PC is positron capture. It is seen that $(\beta^+ + \mathrm{EC})$ contributes negatively to $\dot{Y}_e$ whereas the $(\beta^- + \mathrm{PC})$ rates contribute positively. For the analysis of stellar weak rates, we have utilized the pn-QRPA model with nuclear deformations taken from [33] to determine the $\beta^{\pm}$, EC and PC rates of $^{67-80}$As. We have calculated stellar weak rates that are completely microscopic in nature. The so-called Brink–Axel hypothesis [45] was not applied in our computation for the GT strength distributions of excited states. The stellar weak rates were compiled utilizing the independent-particle model (IPM) for 226 nuclei within $A = 21$–60 [25]. Later, the data were compiled via the same model within $A = 65$–80 [46]. The authors improved their treatment for high-temperature partition functions and adjusted the location of GT centroids from [25] in the updated computation. The computations, referred to as IPM-03 from now on, were based on the Brink–Axel hypothesis. The pn-QRPA stellar rates are calculated and displayed in tables 4 and 5. We display $(\beta^+ + \mathrm{EC})$ and $(\beta^- + \mathrm{PC})$ along with the IPM-03 calculations at all densities and temperatures. It is obvious that the stellar rates increase with core temperature. This happens because a parent state's occupancy probability increases with temperature, making a sufficient contribution to the weak rates. As the density of the star core evolves by orders of magnitude, the

Table 5. Same as table 5 but for sum of (β^- + PC) rates.

		^{67}As		^{68}As		^{69}As	
ρ	T_9	$\lambda^{(\beta^-+\mathrm{PC})}_{\mathrm{pn-QRPA)}}$	$\lambda^{(\beta^-+\mathrm{PC})}_{\mathrm{IPM-03}}$ [46]	$\lambda^{(\beta^-+\mathrm{PC})}_{\mathrm{pn-QRPA}}$	$\lambda^{(\beta^-+\mathrm{PC})}_{\mathrm{IPM-03}}$ [46]	$\lambda^{(\beta^-+\mathrm{PC})}_{\mathrm{pn-QRPA}}$	$\lambda^{(\beta^-+\mathrm{PC})}_{\mathrm{IPM-03}}$ [46]
10^3	3	4.29×10^{-20}	8.24×10^{-17}	1.01×10^{-14}	1.60×10^{-09}	6.82×10^{-15}	4.18×10^{-12}
	10	2.33×10^{-06}	2.88×10^{-05}	2.09×10^{-04}	1.62×10^{-04}	8.18×10^{-05}	1.88×10^{-04}
	30	$5.90\times10^{+00}$	$2.54\times10^{+00}$	$2.82\times10^{+01}$	$8.34\times10^{+00}$	$1.47\times10^{+01}$	$5.46\times10^{+00}$
10^7	3	8.26×10^{-22}	1.61×10^{-18}	1.94×10^{-16}	3.12×10^{-11}	1.31×10^{-16}	8.17×10^{-14}
	10	1.86×10^{-06}	2.30×10^{-05}	1.67×10^{-04}	1.30×10^{-04}	6.52×10^{-05}	1.50×10^{-04}
	30	$5.86\times10^{+00}$	$2.51\times10^{+00}$	$2.82\times10^{+01}$	$8.34\times10^{+00}$	$1.46\times10^{+01}$	$5.42\times10^{+00}$
10^{11}	3	2.75×10^{-60}	5.94×10^{-57}	6.47×10^{-55}	1.15×10^{-49}	4.38×10^{-55}	3.01×10^{-52}
	10	2.28×10^{-18}	2.94×10^{-17}	2.04×10^{-16}	1.67×10^{-16}	7.98×10^{-17}	1.93×10^{-16}
	30	8.04×10^{-04}	3.52×10^{-04}	3.87×10^{-03}	1.19×10^{-03}	2.00×10^{-03}	7.62×10^{-04}

		^{70}As		^{71}As		^{72}As	
ρ	T_9	$\lambda^{(\beta^-+\mathrm{PC})}_{\mathrm{pn-QRPA}}$	$\lambda^{(\beta^-+\mathrm{PC})}_{\mathrm{IPM-03}}$ [46]	$\lambda^{(\beta^-+\mathrm{PC})}_{\mathrm{pn-QRPA}}$	$\lambda^{(\beta^-+\mathrm{PC})}_{\mathrm{IPM-03}}$ [46]	$\lambda^{(\beta^-+\mathrm{PC})}_{\mathrm{pn-QRPA}}$	$\lambda^{(\beta^-+\mathrm{PC})}_{\mathrm{IPM-03}}$ [46]
10^3	3	2.72×10^{-11}	1.88×10^{-07}	7.23×10^{-12}	1.45×10^{-08}	1.79×10^{-08}	9.54×10^{-07}
	10	2.10×10^{-03}	5.36×10^{-04}	3.69×10^{-04}	1.97×10^{-03}	6.59×10^{-03}	1.25×10^{-03}
	30	$8.20\times10^{+01}$	$1.32\times10^{+01}$	$2.10\times10^{+01}$	$8.26\times10^{+00}$	$8.85\times10^{+01}$	$1.23\times10^{+01}$
10^7	3	5.24×10^{-13}	3.68×10^{-09}	1.39×10^{-13}	2.83×10^{-10}	3.75×10^{-10}	1.76×10^{-07}
	10	1.67×10^{-03}	4.29×10^{-04}	2.94×10^{-04}	1.58×10^{-03}	5.25×10^{-03}	1.01×10^{-03}
	30	$8.13\times10^{+01}$	$1.30\times10^{+01}$	$2.08\times10^{+01}$	$8.18\times10^{+00}$	$8.77\times10^{+01}$	$1.21\times10^{+01}$
10^{11}	3	1.74×10^{-51}	1.35×10^{-47}	4.64×10^{-52}	1.04×10^{-48}	3.34×10^{-48}	4.36×10^{-47}
	10	2.05×10^{-15}	5.52×10^{-16}	3.61×10^{-16}	2.04×10^{-15}	6.52×10^{-15}	1.80×10^{-15}
	30	1.12×10^{-02}	1.85×10^{-03}	2.86×10^{-03}	1.15×10^{-03}	1.21×10^{-02}	1.72×10^{-03}

		^{73}As		^{74}As		^{75}As	
ρ	T_9	$\lambda^{(\beta^-+\mathrm{PC})}_{\mathrm{pn-QRPA}}$	$\lambda^{(\beta^-+\mathrm{PC})}_{\mathrm{IPM-03}}$ [46]	$\lambda^{(\beta^-+\mathrm{PC})}_{\mathrm{pn-QRPA}}$	$\lambda^{(\beta^-+\mathrm{PC})}_{\mathrm{IPM-03}}$ [46]	$\lambda^{(\beta^-+\mathrm{PC})}_{\mathrm{pn-QRPA}}$	$\lambda^{(\beta^-+\mathrm{PC})}_{\mathrm{IPM-03}}$ [46]
10^3	3	7.06×10^{-09}	3.81×10^{-06}	1.88×10^{-06}	4.69×10^{-05}	1.45×10^{-06}	5.78×10^{-06}
	10	1.92×10^{-3}	8.36×10^{-03}	2.79×10^{-02}	3.32×10^{-03}	6.10×10^{-03}	1.20×10^{-02}
	30	$4.71\times10^{+01}$	$1.03\times10^{+01}$	$2.11\times10^{+02}$	$1.46\times10^{+01}$	$6.87\times10^{+01}$	$1.38\times10^{+01}$
10^7	3	1.63×10^{-10}	7.44×10^{-08}	9.24×10^{-08}	2.71×10^{-05}	8.63×10^{-08}	6.75×10^{-07}
	10	1.54×10^{-03}	6.68×10^{-03}	2.24×10^{-02}	2.83×10^{-03}	4.90×10^{-03}	9.70×10^{-03}
	30	$4.67\times10^{+01}$	$1.02\times10^{+02}$	$2.09\times10^{+02}$	$1.45\times10^{+01}$	$6.82\times10^{+01}$	$1.37\times10^{+01}$
10^{11}	3	6.49×10^{-49}	2.75×10^{-46}	5.53×10^{-45}	2.57×10^{-46}	3.24×10^{-45}	3.18×10^{-46}
	10	1.90×10^{-15}	8.64×10^{-15}	3.51×10^{-14}	2.16×10^{-14}	7.08×10^{-15}	1.57×10^{-14}
	30	6.43×10^{-03}	1.43×10^{-03}	2.89×10^{-02}	2.09×10^{-03}	9.40×10^{-03}	1.92×10^{-03}

		^{76}As		^{77}As		^{78}As	
ρ	T_9	$\lambda^{(\beta^-+\mathrm{PC})}_{\mathrm{pn-QRPA}}$	$\lambda^{(\beta^-+\mathrm{PC})}_{\mathrm{IPM-03}}$ [46]	$\lambda^{(\beta^-+\mathrm{PC})}_{\mathrm{pn-QRPA}}$	$\lambda^{(\beta^-+\mathrm{PC})}_{\mathrm{IPM-03}}$ [46]	$\lambda^{(\beta^-+\mathrm{PC})}_{\mathrm{pn-QRPA}}$	$\lambda^{(\beta^-+\mathrm{PC})}_{\mathrm{IPM-03}}$ [46]
10^3	3	6.76×10^{-05}	2.01×10^{-03}	4.30×10^{-05}	3.85×10^{-04}	2.88×10^{-03}	2.15×10^{-02}
	10	6.27×10^{-02}	1.26×10^{-02}	1.52×10^{-02}	3.98×10^{-02}	1.80×10^{-01}	6.29×10^{-02}
	30	$2.28\times10^{+02}$	$1.94\times10^{+01}$	$9.10\times10^{+01}$	$1.79\times10^{+01}$	$3.35\times10^{+02}$	$2.55\times10^{+01}$
10^7	3	1.61×10^{-05}	$6.35\times10^{+02}$	1.78×10^{-05}	2.00×10^{-04}	1.90×10^{-03}	1.92×10^{-02}
	10	5.16×10^{-02}	1.15×10^{-02}	1.26×10^{-02}	3.42×10^{-02}	1.55×10^{-01}	5.98×10^{-02}
	30	$2.26\times10^{+02}$	$1.92\times10^{+01}$	$9.02\times10^{+01}$	$1.78\times10^{+01}$	$3.33\times10^{+02}$	$2.53\times10^{+01}$
10^{11}	3	3.90×10^{-42}	1.37×10^{-45}	2.78×10^{-42}	1.91×10^{-45}	2.78×10^{-39}	3.95×10^{-45}
	10	1.76×10^{-13}	3.63×10^{-13}	4.12×10^{-14}	2.13×10^{-13}	1.83×10^{-12}	4.84×10^{-12}
	30	3.13×10^{-02}	3.05×10^{-03}	1.25×10^{-02}	2.52×10^{-03}	4.62×10^{-02}	4.82×10^{-03}

		^{79}As		^{80}As	
ρ	T_9	$\lambda^{(\beta^-+\mathrm{PC})}_{\mathrm{pn-QRPA}}$	$\lambda^{(\beta^-+\mathrm{PC})}_{\mathrm{IPM-03}}$ [46]	$\lambda^{(\beta^-+\mathrm{PC})}_{\mathrm{pn-QRPA}}$	$\lambda^{(\beta^-+\mathrm{PC})}_{\mathrm{IPM-03}}$ [46]
10^3	3	1.11×10^{-03}	1.17×10^{-02}	1.40×10^{-02}	1.14×10^{-01}
	10	4.03×10^{-02}	1.73×10^{-01}	4.15×10^{-01}	2.76×10^{-01}
	30	$1.18 \times 10^{+02}$	$2.34 \times 10^{+01}$	$3.67 \times 10^{+02}$	$3.54 \times 10^{+01}$
10^7	3	7.54×10^{-04}	9.27×10^{-03}	1.14×10^{-02}	1.05×10^{-01}
	10	3.53×10^{-02}	1.62×10^{-01}	3.75×10^{-01}	2.67×10^{-01}
	30	$1.17 \times 10^{+02}$	$2.32 \times 10^{+01}$	$3.64 \times 10^{+02}$	$3.52 \times 10^{+01}$
10^{11}	3	1.29×10^{-39}	5.87×10^{-45}	3.54×10^{-37}	9.91×10^{-45}
	10	3.96×10^{-13}	4.12×10^{-12}	1.31×10^{-11}	5.16×10^{-11}
	30	1.62×10^{-02}	3.41×10^{-03}	5.11×10^{-02}	9.65×10^{-03}

(β^++ EC) rates rise owing to an elevation in electron chemical potential. On the contrary, the (β^-+ PC) rates decrease with increasing core densities due to a significant reduction in the accessible phase space (positrons have a negative degeneracy parameter). The (β^++ EC) rates are only significant at high temperatures and densities. The pn-QRPA rates are up to 22 times greater than the IPM-03 rates because electron and positron pair generation probabilities are maximum at higher temperatures, for example in ^{80}As. Similarly, table 5 displays that the (β^-+ PC) rates make a finite contribution only at high temperatures and low densities. This is due to the Pauli blocking effect at large densities, as well as the substantial reduction in phase space as noted above. It is noted that the IPM-03 rates are lower than the pn-QRPA rates. In the IPM-03 calculation, the sum of the partition function had several states without accompanying weak interaction strengths. The likely cause of the lower rates in the IPM-03 analysis might be the handling of partition functions and the quenching of GT strength.

4. Conclusion

The β-decay properties were analyzed within the context of the pn-QPRA approach. It was found that the computed half-lives were within a factor of 10 of the observed data, and the computed GT distributions agreed with the measured data rather well. The predicted log *ft* values were compared with observed and previously computed data. The present prediction shows a decent agreement with the measured data. The stellar weak interaction rates for As isotopes were computed utilizing a complete microscopic framework, excluding the Brink–Axel hypothesis from the computation of excited state GT distributions. The model-based weak rates exceed the previous predictions (shell model) by a factor of 22. The defined stellar rates might be beneficial for r-process nucleosynthesis predictions and simulations of late-stage star evolution.

Acknowledgments

The authors extend their appreciation to Taif University, Saudi Arabia, for supporting this work through project number (TUDSPP-2024-33). J-U Nabi would like to acknowledge financial support of the Higher Education Commission Pakistan under Grant No. 20-15394/NRPU/R&D/HEC/2021.

Funding

This research was funded by Taif University, Saudi Arabia, Project No. (TU-DSPP-2024-33).

Declaration of competing interest

The authors declare that they have no known competing financial interests or personal relationships that could have appeared to influence the work reported in this paper.

References

[1] Nomura K *et al* 2022 Simultaneous description of β decay and low-lying structure of neutron-rich even- and odd-mass Rh and Pd nuclei *Phys. Rev.* C **106** 064304
[2] Usman S and Mushtaq A 2023 Magnetorotational instability in dense electron–positron–ion plasmas *Sci. Rep.* **13** 15315
[3] Burbidge E M *et al* 1957 Synthesis of the elements in stars *Rev. Mod. Phys.* **29** 547
[4] Woosley S E *et al* 1994 The r-process and neutrino-heated supernova ejecta *Astrophys. J.* **433** 229
[5] Nabi J-U *et al* 2024 Investigation of nuclear structure and β-decay properties of As isotopes *Chin. J. Phys.* **92** 22
[6] Hoff P and Fogelberg B 1981 Properties of strongly neutron-rich isotopes of germanium and arsenic *Nucl. Phys.* A **368** 210
[7] Mazzocchi C *et al* 2013 New half-life measurements of the most neutron-rich arsenic and germanium isotopes *Phys. Rev.* C **87** 034315
[8] Iachello F 1980 The interacting boson–fermion model *Nucl. Phys.* A **347** 51
[9] Álvarez-Rodríguez R *et al* 2004 Deformed quasiparticle random phase approximation formalism for single-and two-neutrino double β decay *Phys. Rev.* C **70** 064309
[10] Minato F, Marketin T and Paar N 2021 β-delayed neutron-emission and fission calculations within relativistic quasiparticle random-phase approximation and a statistical model *Phys. Rev.* C **104** 044321
[11] Kumar A *et al* 2020 Second-forbidden nonunique β-decays of ^{24}Na and ^{36}Cl assessed by the nuclear shell model *Phys. Rev.* C **101** 064304

[12] Irgaziev B F *et al* 2021 Analysis of β^+ decay of ^{13}N nucleus using a modified one-particle approach *Can. J. Phys.* **99** 176

[13] Irgaziev B F *et al* 2021 Application of ANCs for calculation of β^+ decay of ^{17}F nucleus *Nucl. Phys.* A **1021** 122422

[14] Brant S, Yoshida N and Zuffi L 2004 β decay of odd-*A* As to Ge isotopes in the interacting boson–fermion model *Phys. Rev.* C **70** 054301

[15] Sarriguren P 2015 β-decay properties of neutron-rich Ge, Se, Kr, Sr, Ru, and Pd isotopes from deformed quasiparticle random-phase approximation *Phys. Rev.* C **91** 044304

[16] Chen D Z, Fang D L and Bai C L 2021 Impact of finite-range tensor terms in the Gogny force on the β-decay of magic nuclei *Nucl. Sci. Tech.* **32** 74

[17] Bai C L *et al* 2022 Impact of finite-range tensor terms in the Gogny force on the β-decay of magic nuclei *Chin. Phys.* C **46** 114104

[18] Minato F and Bai C L 2013 Impact of tensor force on β-decay of magic and semimagic nuclei *Phys. Rev. Lett.* **110** 122501

[19] Wang Y Z *et al* 2023 A novel power-combination method using a time-reversal pulse-compression technique *Chin. Phys.* C **47** 084101

[20] Shehzadi R, Nabi J-U and Farooq F 2023 Beta decay and electron capture rates of manganese isotopes in astrophysical environments *New Astron.* **98** 101937

[21] Nabi J-U and Böyükata M 2016 β-decay half-lives and nuclear structure of exotic proton-rich waiting point nuclei under rp-process conditions *Nucl. Phys.* A **947** 182

[22] Klapdor-Kleingrothaus H V, Metzinger J and Oda T 1984 β-decay half-lives of neutron-rich nuclei *At. Data Nucl. Data Tables* **31** 81

[23] Staudt A *et al* 1990 Second-generation microscopic predictions of β-decay half-lives of neutron-rich nuclei *At. Data Nucl. Data Tables* **44** 79

[24] Hirsch M *et al* 1993 Microscopic predictions of β^+/EC-decay half-lives *At. Data Nucl. Data Tables* **53** 165

[25] Fuller G M, Fowler W A and Newman M J 1982 Stellar weak interaction rates for intermediate-mass nuclei. II $A = 21$ to $A = 60$ *Astrophys.* J **252** 715

[26] Nabi J-U, Kabir A and Bayram T 2024 Re-analysis of the Gamow–Teller distributions for N = Z nuclei, ^{24}Mg, ^{28}Si, and ^{32}S *Chin. J. Phys.* **87** 797

[27] Nabi J-U *et al* 2021 The nuclear ground-state properties and stellar electron emission rates of ^{76}Fe, ^{78}Ni, ^{80}Zn, ^{126}Ru, ^{128}Pd and ^{130}Cd using RMF and pn-QRPA models *Nucl. Phys.* A **1015** 122278

[28] Kabir A *et al* 2024 Re-analysis of temperature dependent neutron capture rates and stellar β-decay rates of $^{95-98}$Mo *Chin. Phys.* C **48** 094101

[29] Nilsson S G 1955 Binding states of individual nucleons in strongly deformed nuclei *Mat. Fys. Medd. Dan. Vid. Selsk.* **29** 16

[30] Ragnarsson I and Sheline R K 1984 Systematics of nuclear deformations *Phys. Scr.* **29** 385

[31] Kondev F G *et al* 2021 The NUBASE2020 evaluation of nuclear physics properties *Chin. Phys.* C **45** 030001

[32] Ha E, Cheoun M K and Sagawa H 2022 Tensor force effect on pairing correlations for the Gamow–Teller transition in ^{42}Ca, ^{46}Ti, and ^{18}O *Prog. Theor. Exp. Phys.* **4** 043D01

[33] Möller P, Sierk A J, Ichikawa T and Sagawa H 2016 Nuclear ground-state masses and deformations: FRDM(2012) *At. Data Nucl. Data Tables.* **109** 204

[34] Homma H 1996 Systematic study of nuclear β-decay *Phys. Rev.* C **54** 2972

[35] Muto K *et al* 1992 Proton-neutron quasiparticle RPA with separable Gamow–Teller forces *Z. Phys. A Hadrons Nucl.* **341** 407

[36] Hardy J C and Towner I S 2009 Superallowed 0^+- 0^+ nuclear β decays: a new survey with precision tests of the conserved vector current hypothesis and the standard model *Phys. Rev.* C **79** 055502

[37] Nakamura K 2010 Particle Data Group structure functions *J. Phys. G, Nucl. Part. Phys.* **37** 075021

[38] Gove N B and Martin M J 1971 Log-*f* tables for beta decay *At. Data Nucl. Data Tables* **10** 205

[39] Nabi J-U and Klapdor-Kleingrothaus H V 2004 Microscopic calculations of stellar weak interaction rates and energy losses for fp-and fpg-shell nuclei *At. Data Nucl. Data Tables* **88** 237

[40] Nabi J-U and Klapdor-Kleingrothaus H V 1999 Weak interaction rates of sd-shell nuclei in stellar environment calculated in the proton-neutron quasiparticle random phase approximation *At. Data Nucl. Data Tables* **71** 149

[41] Muszynski S and Mark S K 1970 The decay of ^{69}As *Nucl. Phys.* A **142** 459

[42] Yan L *et al* 2002 A decay study of ^{70}As *Appl. Radiat. Isot.* **57** 399

[43] Brookhaven National Nuclear Data Center, http://www.nndc.bnl.gov.

[44] Nomura K 2022 β-decay and evolution of low-lying structure in Ge and As nuclei *Phys. Rev.* C **105** 044306

[45] Ikeda K 1964 Collective excitation of unlike pair states in heavier nuclei *Prog. Theor. Phys.* **31** 434–51

[46] Pruet J and Fuller G M 2003 Estimates of stellar weak interaction rates for nuclei in the mass range $A = 65$–80 *Astrophys. J. Suppl. Ser.* **149** 189